

BINARY-PULSAR TESTS OF STRONG-FIELD GRAVITY AND GRAVITATIONAL RADIATION DAMPING*

GILLES ESPOSITO-FARESE

*GRÉCO, FRE 2435-CNRS, Institut d'Astrophysique de Paris,
98bis boulevard Arago, F-75014 Paris, France
E-mail: gef@iap.fr*

This talk reviews the constraints imposed by binary-pulsar data on gravity theories, focusing on “tensor-scalar” ones which are the best motivated alternatives to general relativity. We recall that binary-pulsar tests are qualitatively different from solar-system experiments, because of nonperturbative strong-field effects which can occur in compact objects like neutron stars, and because one can observe the effect of gravitational radiation damping. Some theories which are strictly indistinguishable from general relativity in the solar system are ruled out by binary-pulsar observations. During the last months, several impressive new experimental data have been published. Today, the most constraining binary pulsar is no longer the celebrated (Hulse-Taylor) PSR B1913+16, but the neutron star-white dwarf system PSR J1141–6545. In particular, in a region of the “theory space”, solar-system tests were known to give the tightest constraints; PSR J1141–6545 is now almost as powerful. We also comment on the possible scalar-field effects for the detection of gravitational waves with future interferometers. The presence of a scalar partner to the graviton might be detectable with the LISA space experiment, but we already know that it would have a negligible effect for LIGO and VIRGO, so that the general relativistic wave templates can be used securely for these ground interferometers.

1. Introduction and solar-system constraints

The most efficient way to test a theory is to contrast its predictions with alternative models. Instead of just confirming or ruling out a particular theory, this method allows us to understand what features have actually been tested, and what kind of observations could be performed to test the remaining features.

The best known example of such an embedding of general relativity in a space of alternatives is the so-called “parametrized post-Newtonian” (PPN) formalism,¹ which describes all possible metric theories of gravity in weak-field conditions, at order $1/c^2$ with respect to the Newtonian interaction. The basic idea was formulated by Eddington,² who wrote the usual Schwarzschild metric in isotropic coordinates, but introduced some phenomenological parameters β^{PPN} and γ^{PPN} in front of the

*Contribution to tenth Marcel Grossmann Meeting, 20–26 July 2003, Rio de Janeiro, Brazil

different powers of the dimensionless ratio Gm/rc^2 :

$$-g_{00} = 1 - 2\frac{Gm}{rc^2} + 2\beta^{\text{PPN}} \left(\frac{Gm}{rc^2}\right)^2 + \mathcal{O}\left(\frac{1}{c^6}\right), \quad (1a)$$

$$g_{ij} = \delta_{ij} \left(1 + 2\gamma^{\text{PPN}} \frac{Gm}{rc^2}\right) + \mathcal{O}\left(\frac{1}{c^4}\right). \quad (1b)$$

General relativity corresponds to $\beta^{\text{PPN}} = \gamma^{\text{PPN}} = 1$, and is in perfect agreement with solar system experiments. At the time of the 10th Marcel Grossmann Meeting (MGX), the tightest published bounds on these parameters were³

$$|\gamma^{\text{PPN}} - 1| < 2 \times 10^{-3}, \quad |\beta^{\text{PPN}} - 1| < 6 \times 10^{-4}. \quad (2)$$

An unpublished⁴ stronger constraint was also known, $|\gamma^{\text{PPN}} - 1| < 4 \times 10^{-4}$, but an impressive new result⁵ has been released two months after MGX:

$$\gamma^{\text{PPN}} - 1 = (2.1 \pm 2.3) \times 10^{-5}. \quad (3)$$

Such bounds tell us that general relativity is basically the only theory consistent with experiment at the first post-Newtonian order. However, they do not constrain higher order terms in metric (1), and the correct theory of gravity might differ significantly from general relativity in strong field conditions. Indeed, if R denotes the radius of a body, the ratio $Gm/Rc^2 \approx 10^{-9}$ for the Earth and $\approx 10^{-6}$ for the Sun, but it reaches ≈ 0.2 for neutron stars, not far from the theoretical maximum of $\frac{1}{2}$ for black holes. Pulsar observations can thus be used to test the strong-field regime of gravity.

2. Binary-pulsar tests

Experiment tells us that isolated pulsars are very stable clocks. A binary pulsar is thus a moving clock, the best tool that one could dream of to test a relativistic theory. Indeed, as the pulsar moves around its companion, the longitudinal Doppler effect modifies its observed spin rate, and we get a stroboscopic information on its orbital velocity. Several parameters characterizing its Keplerian orbit can then be extracted from an analysis of the pulse arrival times. For instance, the time between two maxima of the pulse frequency gives a measure of the orbital period P . One can also extract the eccentricity e , the longitude of periastron ω , and the projected semimajor axis x along the line of sight ($x \equiv \frac{a}{c} \sin i$, where i denotes the inclination of the orbit with respect to the plane of the sky).

If high enough precision is achieved, relativistic corrections can be measured. In particular, if a system is observed long enough, the time derivatives of the Keplerian parameters become available. In the case of the famous Hulse-Taylor binary pulsar **PSR B1913+16**, three such “post-Keplerian” observables have been determined with great accuracy:⁶ (i) the Einstein time delay parameter γ_T , which combines the second-order Doppler effect ($\propto v_A^2/2c^2$, where v_A is the pulsar’s velocity) together with the redshift due to the companion ($\propto Gm_B/r_{AB}c^2$, where m_B

is the companion's mass and r_{AB} the pulsar-companion distance); (ii) the periastron advance $\dot{\omega}$ (relativistic effect of order v^2/c^2); and (iii) the rate of change of the orbital period, \dot{P} , caused by gravitational radiation damping (an effect of order v^5/c^5 in general relativity, but generically of order v^3/c^3 in alternative theories, see below). In any theory of gravity, these three quantities can be computed in terms of the two unknown masses of the pulsar and its companion, and the equations $predictions(m_A, m_B) = observed\ values$ define three curves in the mass plane (or rather three strips if one takes into account experimental uncertainties). This provides $3\ (\text{observables}) - 2\ (\text{unknown masses}) = 1$ test of the theory. If the three strips meet in a small region, there exists a pair of masses consistent with all three observables, and the theory passes the test. If they do not meet, the theory is ruled out. The upper-left panel of Fig. 1 displays this mass plane in the case of general relativity, which is nicely consistent with experimental data within 1σ error bars. This Figure also displays the mass plane for three other binary pulsars which have been timed accurately.

For **PSR B1534+12**, five post-Keplerian observables have been measured:⁷ γ_T , $\dot{\omega}$ and \dot{P} have been described above, whereas $r = Gm_B/c^3$ and $s = \sin i$ denote respectively the “range” (global factor) and the “shape” of the Shapiro time delay. General relativity passes again the $5 - 2 = 3$ tests (at the 1.3σ level for \dot{P} , whose measurement is spoiled by a poorly known Doppler contribution due to the acceleration of the system towards the center of the Galaxy).

The timing measurements of γ_T , $\dot{\omega}$ and \dot{P} for **PSR J1141–6545** are brand-new,⁸ and have been presented at this parallel session PT1 of the MGX meeting (see M. Bailes' contribution to the present proceedings). This binary pulsar was discovered in 1999, and has been quickly recognized as a “strange” system, which triggered several detailed studies. The pulsar is young (~ 1.4 Myr) and thereby nonrecycled, as indicated by its rather slow pulse period (0.4 s). The orbital period is short ($P = 4\text{h } 45\text{min}$), therefore large relativistic effects are expected. The companion is a white dwarf at the 90% confidence level,⁹ but the eccentricity of the orbit ($e = 0.17$) is surprisingly large of such an asymmetrical system. Indeed, almost all known neutron star-white dwarf binaries have a vanishingly small eccentricity. The explanation is that the neutron star was formed *after* the white dwarf in PSR J1141–6545:⁹ Initially, the progenitor's mass was too small to evolve into a neutron star, but it accreted enough matter from its companion, and it finally exploded as a type Ib/c supernova, giving a momentum kick to the newborn neutron star. Before precise timing measurements could be performed, the Keplerian parameters of this system could be determined by an analysis of the pulsar scintillation.¹⁰ This phenomenon, caused by diffraction in the interstellar medium, happens to have a characteristic timescale of minutes for PSR J1141–6545, and this is quick enough to extract orbital information. Indeed, the periodic variation of this scintillation timescale can be interpreted as a consequence of the orbital motion of the pulsar. A fit of the observational data gave two possible orbital solutions,¹⁰ only one of them

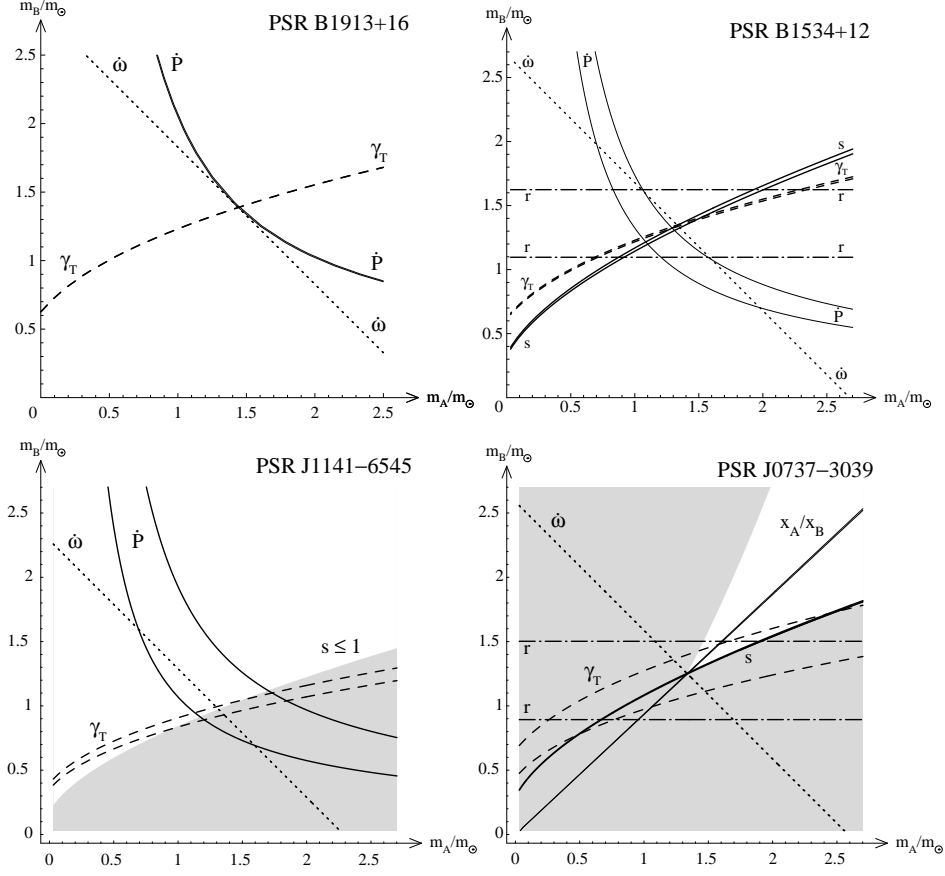


Figure 1. Mass plane (m_A = pulsar, m_B = companion) in general relativity for the four precisely timed binary pulsars. The various strips are consistent at the 1σ level with the timing observables which label them. In the lower two plots, the shaded region corresponds to $|\sin i| > 1$ and is thus excluded.

predicting a pulsar mass $\approx 1.3m_\odot$ consistent with all other known neutron star masses $(1.35 \pm 0.04)m_\odot$. [The fact that it is the lightest known is consistent with the formation scenario summarized above.] The recent timing measurements⁸ of this system nicely confirm (within general relativity) this orbital solution, as shown in the lower-left panel of Fig. 1. Indeed, the intersection of the $\dot{\omega}$ and γ_T curves gives for the masses $m_A/m_\odot = 1.30 \pm 0.02$ and $m_B/m_\odot = 0.986 \pm 0.02$. Kepler’s third law implies the following relation between the inclination angle i , the masses, and the observed quantities P and x :

$$\frac{(m_B \sin i)^3}{(m_A + m_B)^2} = \left(\frac{2\pi}{P}\right)^2 \frac{(xc)^3}{G}. \quad (4)$$

Therefore, once m_A and m_B have been determined thanks to two precise enough post-Keplerian observables, this “mass function” (4) provides the inclination angle

of the orbit. One finds $i > 75^\circ$ at the 1σ level, showing that the orbit is nearly edge on. In such a situation, the mathematical bound^a $|\sin i| \leq 1$ can be used as an extra constraint in the mass plane (m_A, m_B) . The excluded region is shaded in Fig. 1, and we do verify that the intersection of the strips is very close to the limit $\sin i = 1$. This extra constraint will be quite useful below to exclude some alternative theories of gravity. For the above masses and the observed Keplerian parameters of the orbit, general relativity predicts an orbital period derivative $\dot{P} = -3.8 \times 10^{-13}$, nicely consistent with the observed value $\dot{P}^{\text{obs}} = (-4 \pm 1) \times 10^{-13}$, as illustrated also in the lower-left panel of Fig. 1. The 1σ relative errors are still rather large, but since they scale as $t^{-5/2}$, they should reach $\sim 1\%$ by 2010. We will see anyway, in Sec. 4 below, that the present precision is already extremely constraining for alternative theories, and that PSR J1141–6545 is the best system available to test gravity in the strong-field regime.

The timing measurements for **PSR J0737–3039** were released^{11,12} five months after the MGX meeting, but this system is so interesting that I must mention it here. Like PSRs B1913+16 and B1534+12, this is a double neutron star system, but its orbital period is so short ($P = 2\text{h } 27\text{min}$) that huge relativistic effects are expected. [This short orbital period also implies that the system will merge in about 85 Myr, much quicker than any other known neutron star binary; this suffices to increase by a factor 10 the estimated merger rate in our Galaxy,¹¹ and thereby our chances to observe a strong gravitational wave signal in the LIGO/VIRGO interferometers.] The periastron advance could be determined in only a few days of observation, and its value $\dot{\omega} = 17^\circ/\text{yr}$ is much greater than any of the above binary pulsars (the largest being $5.3^\circ/\text{yr}$ for PSR J1141–6545). A careful analysis of the data taken during several months also provided three other post-Keplerian parameters,¹² corresponding to the Einstein (γ_T) and the Shapiro (r and s) time delays. The measure of $s = \sin i$ shows that the orbit is again almost perfectly edge on: $i = (87 \pm 3)^\circ$. Therefore, the mathematical bound $|\sin i| \leq 1$ can again be used as an extra constraint in the mass plane. The shaded region is excluded in the lower-right panel of Fig. 1.^b But the greatest novelty of this system is that the companion has also been observed as a pulsar.¹² Of course, this second pulsar cannot be recycled itself (since only the first formed could accrete matter from its companion), therefore its pulse period is slow (2.8 s) and its observation is not precise enough to provide extra post-Keplerian observables. However, its *Keplerian* orbital data do suffice to give an extra test. Indeed, if x_A and x_B denote the observed projected semi-major axis of both pulsars, the ratio $x_A/x_B = m_B/m_A$ gives a very precise measure of the mass ratio, independently of the theory (and valid at any

^aNote that the Shapiro post-Keplerian parameter $s = \sin i$ has not yet been measured precisely enough to provide another test with PSR J1141–6545 (it should be available within a few months). We are here using only the mathematical fact that it cannot be greater than 1.

^bContrary to PSR J1141–6545, the parameter s is measured for PSR J0737–3039, and the corresponding solid curve should not be considered as the mere boundary of the shaded region. Its width is larger than 1σ error bars.

order in powers of $1/c$, at least in general relativity and tensor-scalar theories). Moreover, if one exchanges the roles of bodies A and B , the mass function (4) and the bound $|\sin i| \leq 1$ give a second excluded region in the mass plane. This is the reason why the white region has got a V shape in the lower-right panel of Fig. 1, and why the shaded (excluded) region covers almost all the plane. This will be quite important to constrain alternative theories of gravity in Sec. 4 below. The orbital period derivative \dot{P} of this double-pulsar system has not yet been determined, but it should be available with reasonable precision within a few months. It will of course provide an extra strip in the mass plane, and thereby an extra test of relativistic gravity in the strong-field regime. Geodetic precession has already been observed in PSRs B1913+16 and B1534+12. This confirms the existence of such an effect, and it can be used to map the emission beam of the pulsar (which gives us information about its structure), but this does not provide an actual test of the theory. On the other hand, the geodetic precession period is predicted to be of about 70 years for both pulsars in PSR J0737–3039, within general relativity. Several years of observation should thus provide an extra test of the theory, which would not have been possible with the other known binary pulsars presented above. Let us finally mention that because this double-pulsar system is almost perfectly edge on, one observes eclipses of the recycled pulsar by its companion, and modulations of the companion’s pulses caused by the energy flux of the recycled pulsar. Therefore, this system will allow us to probe pulsar magnetospheres. Again, this cannot be considered as a test of the gravity theory, but as a powerful new observatory of the physics of neutron stars.

Besides the above four precisely timed binary pulsars, other systems do provide extra tests, even if one does not measure enough post-Keplerian parameters to determine accurately the two masses as in Fig. 1. Indeed, one can use a statistical argument on the pulsar’s mass $m_A \approx 1.35m_\odot$ and the *a priori* arbitrary inclination angle i to predict a probable value for the companion’s mass m_B thanks to the Keplerian “mass function” (4). Then, a single post-Keplerian observable may be compared to the prediction of a theory. For instance, in the neutron star-white dwarf binary **PSR B0655+64**, only an upper bound has been obtained on the orbital period derivative \dot{P} . It is an order of magnitude larger than the prediction of general relativity, therefore this theory is obviously consistent again with experimental data. However, this upper bound suffices to rule out a wide range of alternative theories of gravity, which generically predict a value for \dot{P} several orders of magnitude larger (see Secs. 3 and 4 below). Alternative theories also predict various effects which vanish identically in general relativity, caused by violations of the strong equivalence principle, of local Lorentz invariance or of conservation laws. The experimental upper bounds on such effects therefore just constitute “null tests” for general relativity, but have the capability of constraining other theories. We will mention such an example in Sec. 4 below.

3. Tensor-scalar theories of gravity

As shown in the previous section, several tests of gravity are available in the strong-field regime, and general relativity passes all of them with flying colors. We now wish to embed Einstein's theory into a class of alternatives, in order to understand better which features have been tested, and to compare the probing power of the various tests. A generalization of the PPN formalism to all orders in $1/c^n$ would need an infinite number of parameters. It is much more efficient to restrict our study to the most natural class of alternatives to general relativity, namely "tensor-scalar" theories, in which gravity is mediated by a tensor field ($g_{\mu\nu}$) together with one or several scalar fields (φ). This class of models is privileged for many reasons. (i) They are mathematically consistent field theories, and do not involve any negative-energy mode nor any adynamical field. (ii) The existence of scalar partners to the graviton is predicted by all unified and extra-dimensional theories, notably superstrings. (iii) Scalar fields play a crucial role in modern cosmology, notably to explain the accelerated expansion phases of the universe (inflation, quintessence). (iv) Tensor-scalar models are the only consistent massless field theories able to satisfy the weak equivalence principle (universality of free fall of laboratory-size objects). (v) They are the only known theories satisfying "extended Lorentz invariance", *i.e.*, such that the gravitational physics of subsystems, influenced by external masses, exhibit Lorentz invariance. (vi) They explain the key role played by β^{PPN} and γ^{PPN} in the PPN formalism (the extra 8 parameters introduced by Nordtvedt and Will¹ vanish identically in tensor-scalar theories). (vii) They are general enough to describe many different deviations from general relativity, but simple enough for their predictions to be fully worked out.¹³

In this paper, we will further restrict our study to theories which involve a single scalar field, and which satisfy exactly the weak equivalence principle. Like in general relativity, the action of matter is given by a functional $S_m[\psi_m, \tilde{g}_{\mu\nu}]$ of some matter fields ψ_m (including gauge bosons) and one second-rank symmetric tensor $\tilde{g}_{\mu\nu}$. The difference with general relativity lies in the kinetic term of $\tilde{g}_{\mu\nu}$. Instead of being a pure spin-2 field, it is here a mixing of spin-2 and spin-0 excitations. More precisely, it can be written as $\tilde{g}_{\mu\nu} = \exp[2a(\varphi)]g_{\mu\nu}$, where $a(\varphi)$ is a function of a scalar field φ , and $g_{\mu\nu}$ is the Einstein (spin 2) metric. The action of the theory reads thus

$$S = \frac{c^3}{16\pi G} \int d^4x \sqrt{-g} (R - 2g^{\mu\nu} \partial_\mu \varphi \partial_\nu \varphi) + S_m [\psi_m, e^{2a(\varphi)} g_{\mu\nu}]. \quad (5)$$

[Our signature is $-+++$, R is the scalar curvature of $g_{\mu\nu}$, and g its determinant.]

Our discussion will now be focused on the function $a(\varphi)$, which characterizes the coupling of matter to the scalar field. Let us expand it around the background value of the scalar field, which can be chosen to vanish without loss of generality:

$$a(\varphi) = \alpha_0 \varphi + \frac{1}{2} \beta_0 \varphi^2 + \dots \quad (6)$$

The slope α_0 measures the coupling strength of the linear interaction between matter and the scalar field, β_0 is the quadratic coupling constant of matter to two scalar

lines, *etc.* [A diagrammatic representation is given to label the axes of Figs. 4 and 5 below.] General relativity corresponds to a vanishing function $a(\varphi) = 0$, and Jordan-Fierz-Brans-Dicke theory to a linear function $a(\varphi) = \alpha_0\varphi$, with $\alpha_0^2 = 1/(2\omega_{\text{BD}} + 3)$. As shown below, interesting strong-field effects occur when $\beta_0 \neq 0$, *i.e.*, when $a(\varphi)$ has a nonvanishing curvature.

At the first post-Newtonian order (*i.e.*, when measuring effects of order $1/c^2$ in weak-field conditions), the predictions of tensor-scalar theories depend only on the first two parameters α_0 and β_0 . The effective gravitational constant between two bodies and the Eddington PPN parameters read:

$$G^{\text{eff}} = G(1 + \alpha_0^2), \quad (7a)$$

$$\gamma^{\text{PPN}} - 1 = -2\alpha_0^2/(1 + \alpha_0^2), \quad (7b)$$

$$\beta^{\text{PPN}} - 1 = \frac{1}{2} \frac{\alpha_0\beta_0\alpha_0}{(1 + \alpha_0^2)^2}. \quad (7c)$$

[The factor α_0^2 comes from the exchange of a scalar particle between two bodies, whereas $\alpha_0\beta_0\alpha_0$ comes from a scalar exchange between three bodies.] The solar-system bounds (2)-(3) therefore impose that both α_0^2 and $\alpha_0^2|\beta_0|$ must be small. This implies that the scalar field must be linearly *weakly* coupled to matter. On the other hand, the quadratic coupling strength β_0 is not directly constrained if α_0^2 is small enough, and its sign can also be arbitrary. [Note that $a(\varphi)$ is a coupling function and not a potential for the scalar field, therefore a negative β_0 does not spoil the stability of the field theory.]

At higher post-Newtonian orders $1/c^n$, a simple diagrammatic argument shows that any deviation from general relativity involves at least two factors α_0 , and has the schematic form

$$\text{deviation from G.R.} = \alpha_0^2 \times \left[\lambda_0 + \lambda_1 \frac{Gm}{Rc^2} + \lambda_2 \left(\frac{Gm}{Rc^2} \right)^2 + \dots \right], \quad (8)$$

where $\lambda_0, \lambda_1, \dots$ are constants built from the coefficients α_0, β_0, \dots of expansion (6). Since α_0^2 is experimentally known to be small, we thus expect the theory to be close to general relativity at any order. However, some nonperturbative effects may occur in strong-field conditions: If the compactness Gm/Rc^2 of a body is greater than a critical value, the square brackets of Eq. (8) can become large enough to compensate even a vanishingly small α_0^2 . To illustrate this, let us consider a model for which α_0 vanishes strictly, *i.e.*, which is perturbatively equivalent to general relativity: There is strictly no deviation from general relativity at any order in a perturbative expansion in powers of $1/c$. A parabolic coupling function $a(\varphi) = \frac{1}{2}\beta_0\varphi^2$ suffices for our purpose. At the center of a static body, the scalar field takes a particular value φ_c , and it decreases as $1/r$ outside. The energy of such a scalar field configuration involves two contributions, coming respectively from the kinetic term and from the matter-scalar coupling function in action (5). As a rough

estimate of its value, one can write

$$\text{Energy} \approx \int \left[\frac{1}{2} (\partial_i \varphi)^2 + \rho e^{\beta_0 \varphi^2/2} \right] \approx mc^2 \left(\frac{\varphi_c^2/2}{Gm/Rc^2} + e^{\beta_0 \varphi_c^2/2} \right). \quad (9)$$

When $\beta_0 < 0$, this is the sum of a parabola and a Gaussian, and if the compactness Gm/Rc^2 is large enough, the function $\text{Energy}(\varphi_c)$ has the shape of a Mexican hat, see Fig. 2. The value $\varphi_c = 0$ now corresponds to a local *maximum* of the energy. It is therefore energetically favorable for the star to create a nonvanishing scalar field φ_c , and thereby a nonvanishing “scalar charge” $a'(\varphi_c) = \beta_0 \varphi_c$. This phenomenon is analogous to the spontaneous magnetization of ferromagnets.

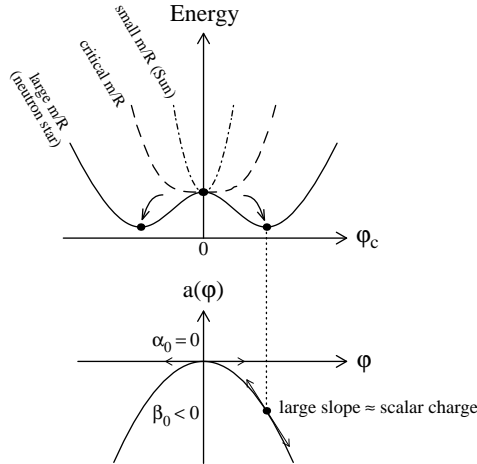


Figure 2. Heuristic argument to explain the phenomenon of “spontaneous scalarization”. When $\beta_0 < 0$ and the compactness Gm/Rc^2 of a body is large enough, it is energetically favorable to create a local scalar field different from the background value. The body becomes thus strongly coupled to the scalar field.

This heuristic argument has been verified by explicit numerical calculations, taking into account the coupled differential equations of the metric and the scalar field, and using various realistic equations of state to describe nuclear matter inside a neutron star.¹⁴ The correct definition of the linear coupling strength between a compact body A and the scalar field reads $\alpha_A \equiv \partial \ln m_A / \partial \varphi_0$. It is plotted in Fig. 3 for the particular model $\beta_0 = -6$. One finds that there exists indeed a “spontaneous scalarization” above a critical mass (whose value decreases as $-\beta_0$ grows). On the other hand, if $\beta_0 > 0$, both the above heuristic argument and the actual numerical calculations show that $|\alpha_A| < |\alpha_0|$. In that case, one finds that neutron stars are even less coupled to the scalar field than solar-system bodies.

The scalar charge α_A enters the predictions of the theory in the same way as α_0 in weak-field conditions. For instance, the effective gravitational constant between

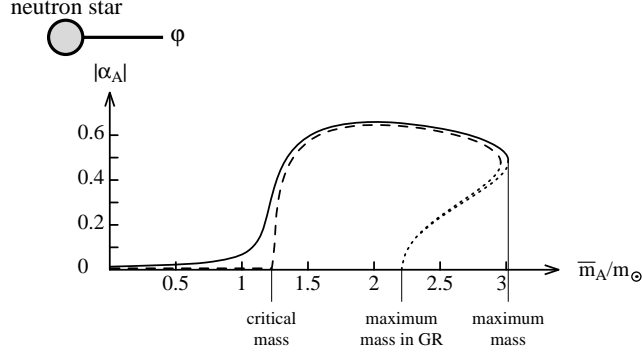


Figure 3. Scalar charge α_A versus baryonic mass \bar{m}_A , for the model $a(\varphi) = -3\varphi^2$ (*i.e.*, $\beta_0 = -6$). The solid line corresponds to the maximum value of α_0 allowed by the Eqs. (2), and the dashed line to $\alpha_0 = 0$. The dotted lines correspond to unstable configurations of the star.

two bodies A and B reads

$$G_{AB}^{\text{eff}} = G(1 + \alpha_A \alpha_B), \quad (10)$$

instead of Eq. (7a). Similarly, the strong-field analogues of the Eddington parameters γ^{PPN} and β^{PPN} involve products of α_A , α_B , $\beta_A \equiv \partial\alpha_A/\partial\varphi_0$ and β_B , instead of α_0 and β_0 as in Eqs. (7). Since the scalar charge $\alpha_A \approx 0.6$ in the model of Fig. 3, one thus expects deviations by $\sim 35\%$ from some general relativistic predictions. Moreover, the quadratic coupling strength β_A can take very large numerical values near the critical mass, like the magnetic susceptibility of ferromagnets. Therefore, even larger deviations from general relativity are found when the mass of a neutron star happens to be close to the critical one. An even more spectacular phenomenon occurs for the quantity $\alpha_B \partial \ln I_A / \partial \varphi_0$, involved in the post-Keplerian observable^c γ_T . Indeed, when $\beta_0 < 0$, this quantity blows up as $\alpha_0 \rightarrow 0$: Paradoxically, a theory which is closer to general relativity in weak-field conditions predicts larger deviations in the strong-field regime! On the other hand, when $\beta_0 > 0$, strong-field predictions are even closer to those of general relativity than in the solar system.

The post-Keplerian observable which is the most affected by the presence of a scalar partner to the graviton is the orbital period derivative \dot{P} . Indeed, the energy flux carried out by gravitational waves is of the form

$$\begin{aligned} \text{Energy flux} = & \left\{ \frac{\text{Quadrupole}}{c^5} + \mathcal{O}\left(\frac{1}{c^7}\right) \right\}_{\text{helicity } 2} \\ & + \left\{ \frac{\text{Monopole}}{c} + \frac{\text{Dipole}}{c^3} + \frac{\text{Quadrupole}}{c^5} + \mathcal{O}\left(\frac{1}{c^7}\right) \right\}_{\text{helicity } 0}. \end{aligned} \quad (11)$$

The first curly brackets contain the prediction of general relativity. The second ones contain the extra contributions predicted in tensor-scalar theories. The powers of

^cThis expression enters γ_T because the inertia moment of the pulsar, I_A , is modified by the presence of a companion at a varying distance.

$1/c$ give the orders of magnitude of the different terms. In particular, the monopolar and dipolar helicity-0 waves are generically expected to be much larger than the usual quadrupole of general relativity. However, the scalar monopole has the form

$$\frac{\text{Monopole}}{c} = \frac{G}{c} \left\{ \frac{\partial(m_A \alpha_A)}{\partial t} + \frac{\partial(m_B \alpha_B)}{\partial t} + \mathcal{O}\left(\frac{1}{c^2}\right) \right\}^2, \quad (12)$$

and it reduces to order $\mathcal{O}(1/c^5)$ if the stars A and B are at equilibrium, $\partial_t(m_A \alpha_A) = 0$, which is the case for all binary pulsars quoted in Sec. 2 above. However, this monopolar term would be huge in the case of a collapsing star, for instance. The dipole has the form

$$\frac{\text{Dipole}}{c^3} = \frac{G}{3c^3} \left(\frac{G_{AB} m_A m_B}{r_{AB}^2} \right)^2 (\alpha_A - \alpha_B)^2 + \mathcal{O}\left(\frac{1}{c^5}\right), \quad (13)$$

and is usually much larger than a quadrupole of order $1/c^5$. For instance, in a pulsar-white dwarf binary, the pulsar's scalar charge α_A may be of order unity, like in Fig. 3 above, whereas the weakly self-gravitating white dwarf has a very small scalar charge $\alpha_B \approx \alpha_0$, constrained by Eqs. (3) and (7b). On the other hand, in a double-neutron star system, one expects $m_A \approx m_B$ and therefore $\alpha_A \approx \alpha_B$, so that this dipolar contribution is considerably reduced (but may still be large with respect to the usual quadrupole of general relativity). Indeed, a dipole is a vector in space, and two strictly identical stars do not define a preferred orientation.

It should be noted that even within Brans-Dicke theory, *i.e.*, for a linear coupling function $a(\varphi) = \alpha_0 \varphi$, the dipolar contribution (13) does not vanish identically. Indeed, in that case, one can show that $\alpha_A = \alpha_0(1 - 2s_A)$, where $s_A \approx Gm/Rc^2$ is the compactness of the star, so that $(\alpha_A - \alpha_B)^2 = 4\alpha_0^2(s_A - s_B)^2$. The dipolar contribution is thus proportional to the experimentally small factor $\alpha_0^2 = 1/(2\omega_{\text{BD}} + 3)$, but it does not vanish, and can still be larger than the usual quadrupole if $\alpha_0^2 > v^2/c^2 \sim 10^{-6}$. Note also that because $s_A \approx Gm/Rc^2$, this dipole (13) is formally of order $\mathcal{O}(G^3/c^7)$, so that one could not have obtained it by a naive calculation at linear order in G . It is however crucial to take it into account, because it is numerically of order $\mathcal{O}(G/c^3)$ since $Gm/Rc^2 \approx 0.2$ for a neutron star.

4. Experimental constraints on tensor-scalar theories

We saw in the previous section that solar-system experiments probe only the first two coefficients α_0 and β_0 of the matter-scalar coupling function (6). On the other hand, the strong-field predictions do depend on the full shape of this function. In order to compare easily the different constraints, we will restrict our study to a strictly parabolic function $a(\varphi) = \alpha_0 \varphi + \frac{1}{2} \beta_0 \varphi^2$. Figure 4 displays the known constraints¹⁴ at the time of the previous Marcel Grossmann meeting MG9, three years ago. Since the physics does not depend on the sign of α_0 , only a half plane $(|\alpha_0|, \beta_0)$ is drawn. Each point on this figure represents a tensor-scalar theory. General relativity is at the origin $\alpha_0 = \beta_0 = 0$, Brans-Dicke theory is on the

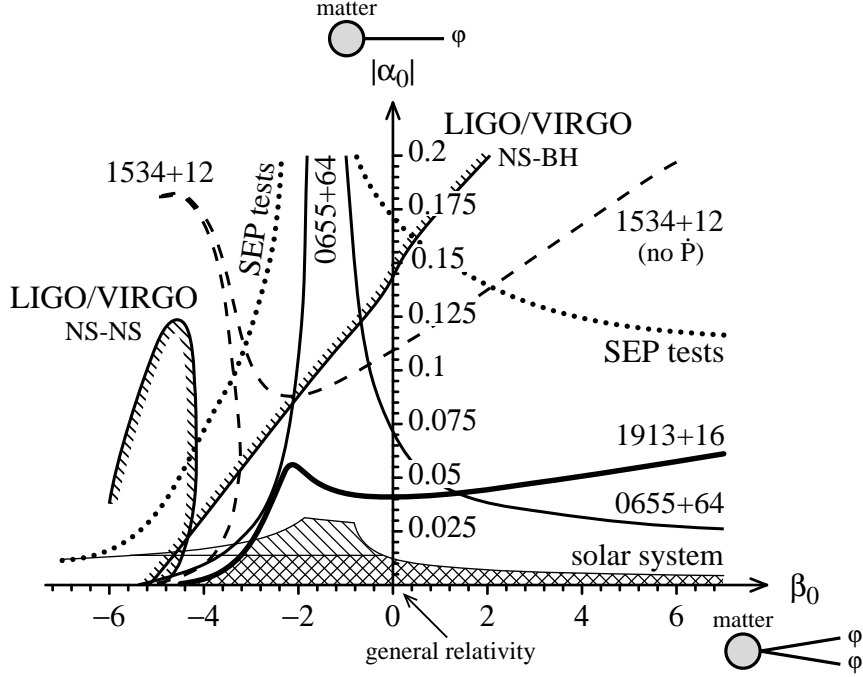


Figure 4. Constraints on generic tensor-scalar theories imposed by solar-system experiments, classic binary-pulsar tests, and future detections of inspiralling binaries with laser interferometers. The hatched region is allowed by all the tests. The doubly hatched one is also consistent with VLBI data.⁴

vertical axis $\beta_0 = 0$, and the horizontal axis $\alpha_0 = 0$ corresponds to theories which are perturbatively equivalent to general relativity (see Sec. 3 above). For each theory $(|\alpha_0|, \beta_0)$, the mass planes of the various binary pulsars can be plotted like in Fig. 1, and if the different strips do not have a common intersection, the theory is ruled out. The allowed theories lie under and to the right of the various curves.

The thin solid line labeled “solar system” corresponds to the bounds (2), and the unpublished limit provided by very long baseline interferometry⁴ (VLBI) is materialized by a thin horizontal line. As discussed in the previous section, they impose a very small matter-scalar linear coupling strength α_0 , but do not constrain the quadratic coupling β_0 if α_0 is small enough.

On the other hand, binary pulsars impose $\beta_0 > -4.5$, even for a vanishingly small α_0 . As discussed in the previous section, this constraint is due to the spontaneous scalarization of neutron stars, which occurs when $-\beta_0$ is large enough. Equations (7) allow us to rewrite this inequality in terms of the Eddington parameters β^{PPN} and γ^{PPN} , which are both consistent with 1 in the solar system. One finds

$$\frac{\beta^{\text{PPN}} - 1}{\gamma^{\text{PPN}} - 1} < 1.1. \quad (14)$$

The singular (0/0) nature of this ratio vividly expresses why such a conclusion could not be obtained in weak-field experiments, and underlines that binary-pulsar tests are qualitatively different.

This bound is mainly due to the Hulse-Taylor binary pulsar **PSR B1913+16**. For **PSR B1534+12**, whose orbital period derivative \dot{P} is not very well known, we have plotted the constraints imposed only by the four post-Keplerian observables $\dot{\omega}$, γ_T , r and s . This gives much weaker constraints than PSR B1913+16, but this is nevertheless a very important test because it does not depend on the radiative structure of the theory. Taking into account the measured value of \dot{P} removes the horn-shaped region at the top-left of the dashed line.

The second most constraining system is the neutron-star white dwarf **PSR B0655+64**, although it has not been timed precisely enough to determine the two component masses, and that only an upper experimental bound on its orbital period derivative \dot{P} is known. Indeed, even by choosing conservative values for the two masses, such an asymmetrical system loses too much energy through dipolar scalar waves in most scalar-tensor theories, see Eq. (13).

Equation (10) above tells us that the acceleration of a neutron star A towards the center C of the Galaxy is proportional to $(1 + \alpha_A \alpha_C)$, whereas a white dwarf B is accelerated with a force $\propto (1 + \alpha_B \alpha_C)$. Since $\alpha_A \neq \alpha_B$ in general, there is a violation of the strong equivalence principle (**SEP**). This causes a polarization of the orbit of a neutron star-white dwarf system towards the Galaxy center, analogous to the Stark effect in electromagnetism. More precisely, the eccentricity vector \mathbf{e} of the orbit is the sum of a fixed vector \mathbf{e}_F directed towards the Galaxy center (proportional to the difference of the accelerations of the two bodies) and of a rotating vector $\mathbf{e}_R(t)$ corresponding to the usual relativistic periastron advance at angular velocity $\dot{\omega}_R$. Several asymmetric systems of this kind (such as PSRs 1713+0747, 2229+2643, 1455–3330) happen to have a very small eccentricity. The only explanation would be that the rotating vector $\mathbf{e}_R(t)$ is precisely canceling the fixed contribution \mathbf{e}_F at the time of our observation: $\mathbf{e}_F + \mathbf{e}_R(t) \approx \mathbf{0}$. However, this is very improbable if the system is old enough, and one can use a statistical argument to constrain the space of theories. Moreover, by considering several such systems, the probability that they have simultaneously a small eccentricity is the product of the already small individual probabilities. The allowed tensor-scalar theories lie between the two (approximate) dotted lines. This test is much less constraining than the others because the Galaxy is not compact enough to be spontaneous scalarized, therefore its scalar charge $\alpha_C \approx \alpha_0$ is small, and the difference of the accelerations $\propto (\alpha_A - \alpha_B)\alpha_C \approx (\alpha_A - \alpha_0)\alpha_0$ is small too.

To detect the gravitational wave signal from an inspiralling binary with the **LIGO/VIRGO** interferometers, one will perform a matched filter analysis of the signal, using the gravitational wave templates predicted by general relativity. In tensor-scalar theories, the waveforms are very different, because of the extra contributions of the scalar waves to the energy loss, Eq. (11). Therefore, the ac-

tual detection of an inspiralling binary with the general relativistic templates will constrain the magnitude of the scalar contributions. The hatched curve labeled “LIGO/VIRGO NS-BH” displays the region of the theory space which would be excluded if a $1.4m_\odot$ neutron star– $10m_\odot$ black hole system is detected with a signal to noise ratio $S/N = 10$ (the excluded region lie on the hatched side). The detection of a double neutron star system with masses similar to those of PSR B1913+16 would exclude the bubble of theories labeled “LIGO/VIRGO NS-NS”. As we can see on Fig. 4, these regions are *already* excluded by binary-pulsar tests. Therefore, we can conclude that the general relativistic wave template do suffice for these interferometers: Even if there exists a scalar partner to the graviton, we anyway already know that it is too weakly coupled to matter to change significantly the waveforms. This is a good news, because the inclusion of possible scalar contributions would have considerably slowed the data analysis. On the other hand, it has been proven¹⁵ that the LISA space interferometer could still be sensitive to scalar-field effects. Indeed, the detection of a neutron star inspiralling a $1000m_\odot$ black hole would probe values of $|\gamma^{\text{PPN}} - 1|$ as small as 4×10^{-6} , *i.e.*, an order of magnitude tighter than the best present bounds (3) [or a factor 3 tighter for the matter-scalar coupling strength α_0]. However, we will see below that the binary pulsar PSR J1141–6545 will probably probe similar values of $|\gamma^{\text{PPN}} - 1|$ around 2010. Therefore, it may not be necessary to start including scalar corrections to the wave templates for LISA: This binary pulsar should tell us, just before the launch of the LISA mission, whether there is or not a scalar contribution at this order.

The constraints imposed by the recently timed **PSR J1141–6545** are much tighter than the previous ones, and we plot them as a dot-dashed curve in Fig. 5. We present here preliminary results, which will be refined in a forthcoming publication.¹⁶ Note that the vertical scale of this Figure has been expanded by a factor 2 with respect to Fig. 4. To ease the comparison of these two Figures, we have repeated in Fig. 5 the curves corresponding to PSR B1913+16 and to solar-system constraints. The reason why PSR J1141–6545 is so constraining is because this is an asymmetrical system, composed of a neutron star and a white dwarf. Therefore, like PSR B0655+64 above, it generically emits a large amount of dipolar scalar waves, which are inconsistent with the small measured value of its orbital period derivative \dot{P} . The lower-left panel of Fig. 1 shows that the experimental precision on this quantity is not very good yet. However, this is already much better than the mere upper bound on \dot{P} that we knew for PSR B0655+64.

Like all binary pulsars, PSR J1141–6545 excludes tensor-scalar theories corresponding to $\beta_0 < -4.5$, even for a strictly vanishing α_0 . This is again due to the phenomenon of spontaneous scalarization described in Sec. 3. But it is quite remarkable that this system is also very constraining in the region of positive β_0 ’s. It is almost as powerful as the previously known solar-system bounds (2). This may seem paradoxical, because we saw that when $\beta_0 > 0$, strongly self-gravitating bodies are much more weakly coupled to the scalar field than matter in the solar

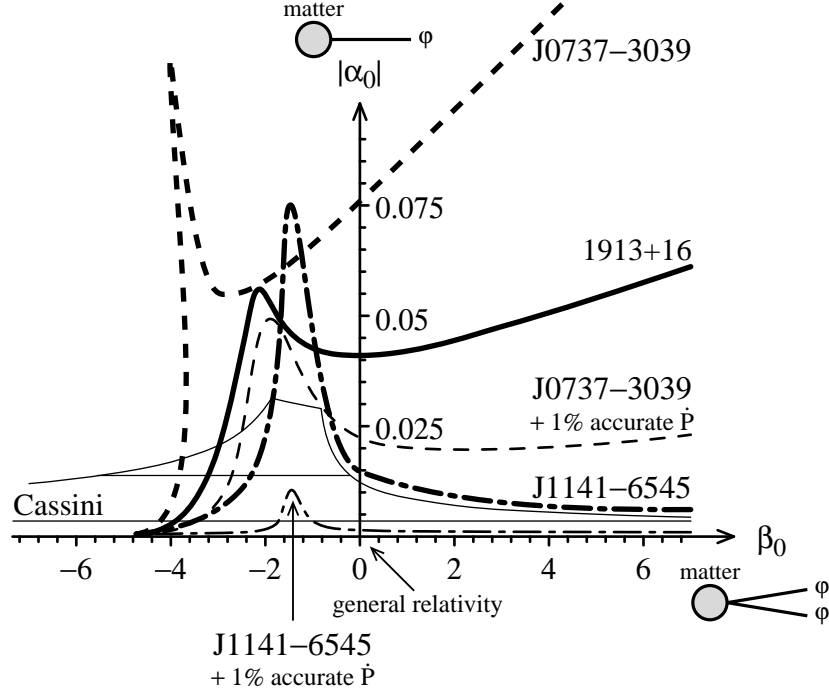


Figure 5. Constraints imposed on the theory space by the two recently timed binary pulsars PSR J1141–6545 and J0737–3039. The thinner lines display the constraints which will be reached when the orbital period derivative \dot{P} is determined with 1% accuracy. We also display here the impressive solar-system constraint (3) obtained recently from the observation of the Cassini spacecraft near solar conjunction.⁵

system. The reason why this binary pulsar anyway provides a powerful test in this region of the theory plane is again its asymmetry. Indeed, the pulsar’s scalar charge is exponentially small, $|\alpha_A| \ll |\alpha_0|$, whereas the weakly self-gravitating white dwarf companion has a standard (background) scalar charge $\alpha_B \approx \alpha_0$. Therefore, the dipolar radiation term (13), proportional to $(\alpha_A - \alpha_B)^2 \approx \alpha_0^2$, is non negligible, and the small observed value of \dot{P} is still constraining. The asymptotic limit of the bound on $|\alpha_0|$ for $\beta_0 \rightarrow +\infty$ can also be estimated analytically,^d by imposing that the dipolar contribution (13) is smaller than the experimental error $\Delta\dot{P}$. One finds

$$\alpha_0^2 < \frac{96}{5} \left(\frac{2\pi G(m_A + m_B)}{Pc^3} \right)^{2/3} \frac{1 + \frac{73}{24}e^2 + \frac{37}{96}e^4}{(1 + \frac{e^2}{2})(1 - e^2)} \left| \frac{\Delta\dot{P}}{\dot{P}} \right| \approx 5 \times 10^{-5} \left| \frac{\Delta\dot{P}}{\dot{P}} \right|. \quad (15)$$

With the present uncertainty on $\dot{P}^{\text{obs}} = (-4 \pm 1) \times 10^{-13}$, this gives $|\alpha_0| < 0.004$

^dOur formal limit $\beta_0 \rightarrow +\infty$ actually means $\beta_0 \sim 10$ or 30 , but for extremely large values of this parameter, the “de-scalarization” phenomenon would affect the white dwarf too, and the constraints would thus weaken.

for $\beta_0 \rightarrow +\infty$, consistently with the curve plotted in Fig. 5. As mentioned in Sec. 2, the precision on \dot{P} should reach 1% by the end of the decade. This would give an asymptotic bound $|\alpha_0| < 7 \times 10^{-4}$ for $\beta_0 \rightarrow +\infty$, corresponding to $|\gamma^{\text{PPN}}| < 10^{-6}$, more than one order of magnitude tighter than the recent limit (3). This estimate is confirmed by our numerical plot, in Fig. 5, of the constraints that PSR J1141–6545 will impose when this precision is reached. Of course, a detailed analysis of the possible sources of noise will be necessary then, notably of the tidal effects on the white dwarf, and of the Doppler contribution due to the acceleration of the system towards the center of the Galaxy.

To give the reader a better feeling of the above limits, we display in Fig. 6 the mass plane for PSR J1141–6545 in four different scalar-tensor theories. The

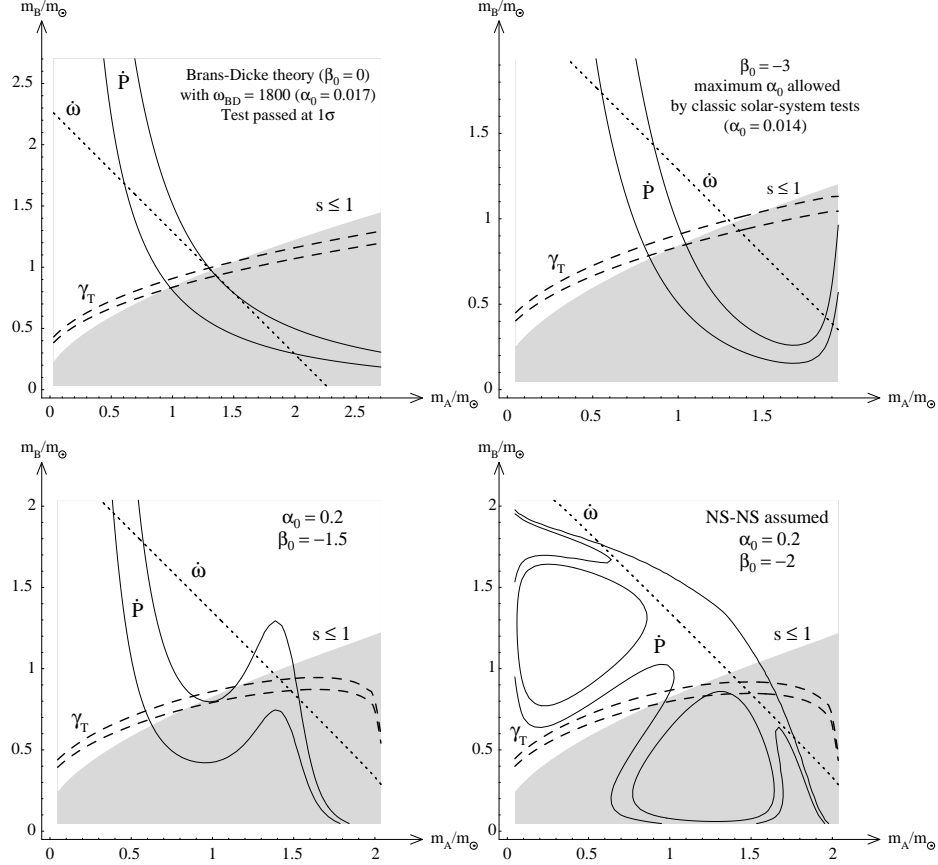


Figure 6. Mass plane (m_A = pulsar, m_B = companion) for PSR J1141–6545 in four different tensor-scalar theories of gravity. Only the upper-left plot corresponds to an allowed model (at the 1σ level). In the lower-right plot, the system is assumed to be a double-neutron star system.

upper-left plot corresponds to Brans-Dicke theory, *i.e.*, to a linear matter-scalar

coupling function $a(\varphi) = \alpha_0 \varphi$, with $\alpha_0^2 = 1/(2\omega_{\text{BD}} + 3)$. The value of α_0 has been fine tuned to pass the test exactly at the 1σ level. This theory corresponds thus to the intersection of the thick dot-dashed curve of Fig. 5 with the vertical axis. The corresponding limit $|\gamma^{\text{PPN}}| < 6 \times 10^{-4}$ ($\Leftrightarrow \omega_{\text{BD}} > 1800$) is not far from the unpublished VLBI constraint,⁴ as can be also directly seen on Fig. 5. Note that in Fig. 6, the \dot{P} strip has been significantly displaced with respect to its location in general relativity (lower-left panel of Fig. 1).

The upper-right panel of Fig. 6 displays the mass plane for a theory which was allowed by *all* experimental data at the time of the MGX conference, but which is violently ruled out (by 5σ) by PSR J1141–6545. Indeed, the three strips do not have any common intersection. This illustrates that this binary pulsar is much more constraining than the others, at least in the privileged class of tensor-scalar theories. However, the subsequent solar-system bound (3) does even better.

The lower-left panel of Fig. 6 provides an example of a theory in which the three strips γ_T , $\dot{\omega}$ and \dot{P} do have a common intersection, but it is located in the shaded region corresponding to $|\sin i| > 1$ (see Sec. 2 above). [The lower-right panel gives another example.] Therefore, in such a case, this (Keplerian) mathematical constraint becomes crucial. If the inequality $|\sin i| \leq 1$ is not taken into account, the bump of the thick dot-dashed curve blows up to very large values of $|\alpha_0|$, in Fig. 5. Note however that such theories are anyway ruled out by solar-system experiments.

The lower-right panel of Fig. 6 illustrates the strange shapes that the curves can take in some theories. Here, the topology of the \dot{P} “strip” has even changed. Note also that the intersection of the strips corresponds to masses which are significantly different from those obtained in general relativity (lower-left panel of Fig. 1). Therefore, it would be inconsistent to use the masses obtained within general relativity to compute the predicted \dot{P} in another theory. Obviously, all the strips must be computed within the *same* theory, and the binary-pulsar test is passed if they have a common intersection, even if its location differs from that obtained in general relativity. Contrary to the other three mass planes, the lower-right one has been computed while assuming that PSR J1141–6545 is a double-neutron star system. This is excluded at the 90% level by the formation scenario⁹ of this system. However, it remains instructive to study the dependence of the constraints on the nature of the companion. If it were a neutron star, the system would be much more symmetric ($\alpha_A \approx \alpha_B$), therefore the dipolar contribution (13) to the energy flux would be much lower, and the observed value of \dot{P} less constraining. We did plot the corresponding bounds in the theory plane ($|\alpha_0|, \beta_0$), but we do not display them here to clarify the Figures. It suffices to mention that PSR J1141–6545 would give constraints similar to those of PSR B0655+64 if it were a double neutron star system (see Fig. 4).

Let us come back to Figure 5 above, where we also plotted as dashed lines the bounds imposed by the double pulsar **PSR J0737–3039**, at present and when a 1% accurate \dot{P} is available. Curiously enough, in spite of the great precision of the

measures, and although the mass ratio $m_A/m_B = 1.07$ is tightly fixed independently of the theory, this system appears not to be extremely constraining for scalar-tensor theories. When a 1% accurate \dot{P} is measured, it will of course provide a much stronger test, and become more constraining than the Hulse-Taylor binary pulsar PSR B1913+16. However, it pales in comparison with the neutron star-white dwarf binary PSR J1141–6545, even with its present large uncertainties on \dot{P} . The reason is that the two components of PSR J0737–3039 are neutron stars with similar scalar charges, and therefore that its dipolar radiation (13) is weak. One may also wonder why at present, without any observed \dot{P} , the constraints imposed by this system are so loose, as compared to those of PSR B1913+16. The reason seems to be that the five observed functions of the masses (*cf.* the lower-left panel of Fig. 1) depend only weakly on the presence of a scalar field. Two of them, r and x_A/x_B , are even totally insensitive to it. Only γ_T can vary a lot when spontaneous scalarization occurs (because of the blowing contribution $\alpha_B \partial \ln I_A / \partial \varphi_0$, see Sec. 3), but this post-Keplerian parameter happens to have still large experimental uncertainties.

Figure 7 displays the mass plane (m_A, m_B) for PSR J0737–3039 within two tensor-scalar theories. The left panel illustrates that this system has the capabil-

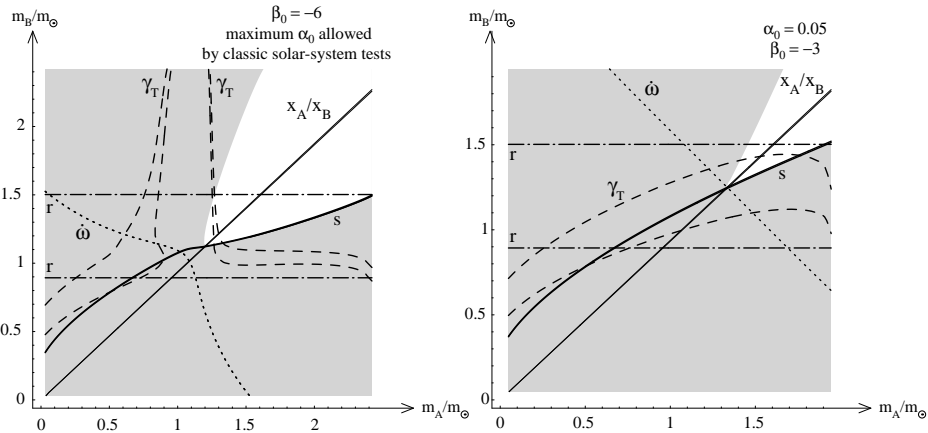


Figure 7. Mass plane (m_A = pulsar, m_B = companion) for PSR J0737–3039 in two different tensor-scalar theories of gravity. The left plot corresponds to a theory which is ruled out by all binary-pulsar tests, including the present one. The theory considered in the right panel passes the present test, although it is ruled out by several other binary pulsars.

ity of ruling out some models. As shown in Fig. 5, it forbids all theories with $\beta_0 < -4.5$, even for a strictly vanishing α_0 , *i.e.*, even if the theory is strictly indistinguishable from general relativity in the weak-field conditions of the solar system. This property is shared by all binary pulsars. They exhibit similar deformations of the various strips in the mass plane, as soon as $-\beta_0$ is large enough. Notice in particular the characteristic shape of the γ_T strip, caused by the spontaneous scalarization of neutron stars.

On the contrary, the right panel of Fig. 7 illustrates that this system is presently less constraining than several other binary pulsars. Indeed, the model $\alpha_0 = 0.05$, $\beta_0 = -3$ is inconsistent with PSRs B1913+16, B0655+64, and J1141–6545, but it passes the test for the double pulsar J0737–3039. This mass plane confirms that the five observables are weakly dependent on the scalar field. The largest deformation occurs for the γ_T strip, with respect to general relativity (lower-right panel of Fig. 1), but its width is large enough for the test to be passed. Of course, such a model will be also ruled out by this double pulsar J0737–3039 once its \dot{P} is measured with reasonable precision.

Let us recall that this double pulsar will anyway provide brand new tests of relativistic gravity, as well as very important information about the astrophysics of pulsars, although its discriminating power seems rather weak at present in the framework of tensor-scalar theories. Moreover, if the new tests happen not to be passed by general relativity, one can already bet that no tensor-scalar theory will be able to pass them either. Therefore, this system has actually the capability of ruling out the best class of gravity theories as a whole. On the other hand, if general relativity passes the new tests, as we expect, this double pulsar will not teach us much about tensor-scalar models.

5. Conclusions

Binary pulsars are ideal tools for testing relativistic gravity in the strong field regime. In the most natural class of alternatives to general relativity, tensor-scalar theories, their probing power has been shown to be qualitatively different from weak-field experiments: They have the capability of testing theories which are strictly equivalent to general relativity in the solar system.

Two fantastic binary pulsars have been timed recently. The double pulsar J0737–3039 promises to be the best laboratory for testing general relativity itself, and for studying the physics of pulsars. On the other hand, the neutron star-white dwarf system PSR J1141–6545 is by far the most constraining binary pulsar known at present, because its asymmetry implies that it generically emits strong dipolar gravitational waves in scalar-tensor theories. It is already almost as constraining as solar-system tests even in the region of positive β_0 's, where binary pulsars never competed with weak-field experiments up to now. It should probe values of the Eddington parameter $|\gamma^{\text{PPN}} - 1| \sim 10^{-6}$ by the end of the decade, *i.e.*, more than one order of magnitude better than present solar-system limits.

Binary pulsars are so precise that they already exclude the models which would have predicted some significant scalar-field contributions to the gravitational wave templates necessary for LIGO and VIRGO. Therefore, one may use securely the general relativistic templates for these interferometers. It is still possible that such scalar-field effects be detectable with the LISA space interferometer, but binary pulsars will probably give us tighter bounds before it is launched.

References

1. C.M. Will, *Theory and Experiment in Gravitational Physics*, Cambridge University Press (1993).
2. A.S. Eddington, *The Mathematical Theory of Relativity*, Cambridge University Press (1923).
3. C.M. Will, *Living Rev. Rel.* **4**, 4 (2001), gr-qc/0103036.
4. T.M. Eubanks *et al.*, *Bull. Am. Phys. Soc.*, Abstract No. K 11.05 (1997), unpublished; draft available at ftp://casa.usno.navy.mil/navnet/postscript/prd_15.ps (1999); S.S. Shapiro *et al.*, *Phys. Rev. Lett.* (2004), in press.
5. B. Bertotti, L. Iess, and P. Tortora, *Nature* **425**, 374 (2003).
6. J.M. Weisberg and J.H. Taylor, *ASP Conference Proceedings* **302**, 93 (2003), astro-ph/0211217.
7. I. Stairs *et al.*, *Astrophys. J.* **581**, 501 (2002), astro-ph/0208357.
8. M. Bailes *et al.*, *Astrophys. J.* **595**, L49 (2003), astro-ph/0307468.
9. T.M. Tauris and T. Sennels, *Astron. Astrophys.* **355**, 236 (2000), astro-ph/9909149.
10. S.M. Ord, M. Bailes, and W. van Straten, *Astrophys. J.* **574**, L75 (2002), astro-ph/0204421.
11. M. Burgay *et al.*, *Nature* **426**, 531 (2003), astro-ph/0312071.
12. A.G. Lyne *et al.*, submitted to *Science* (2004), astro-ph/0401086.
13. T. Damour and G. Esposito-Farese, *Class. Quantum Grav.* **9**, 2093 (1992).
14. T. Damour and G. Esposito-Farese, *Phys. Rev. Lett.* **70**, 2220 (1993); *Phys. Rev. D* **54**, 1474 (1996), gr-qc/9602056; *Phys. Rev. D* **58**, 042001 (1998), gr-qc/9803031.
15. P.D. Scharre and C.M. Will, *Phys. Rev. D* **65**, 042002 (2002), gr-qc/0109044.
16. T. Damour and G. Esposito-Farese, in preparation (2004).